Buckling of Ultralight Ladder-Type Coilable Space Structures

Fabien Royer* and Sergio Pellegrino†

California Institute of Technology,1200 E California Blvd.,Pasadena, CA 91125

We analyse the buckling and post-buckling behavior of ultralight ladder-type coilable structures for space solar power applications. The structures are composed of thin-shell longitudinal elements connected by thin rods, which can be flattened and packaged efficiently. Rather than relying on an eigenvalue based analysis, this paper presents an alternative approach to thin-shell buckling based on recent work on the stability of cylindrical and spherical shells. The stability of ladder-type structures loaded by normal pressure is studied using a probe that locally displaces the structure and a stability landscape for the structure is plotted. This landscape plot gives insight into the structure's buckling, post-buckling, and sensitivity to disturbances.

I. Introduction

We are currently investigating structural architectures for ultralight, coilable space structures suitable for large, deployable, flat spacecraft[1] in the Space-based Solar Power Project (SSPP)at Caltech. In the deployed configuration, each spacecraft measures up to 60 m $\times$ 60 m in size and is composed of ultralight ladder-type coilable strips of equal width, arranged to form a square, and each strip supports many photovoltaic and power transmission tiles. The structure is described in a previous paper[5] and in figure 1. The whole structure is folded and packaged using a folding pattern derived from origami.[2] Scaled laboratory prototypes of this structural concept have been built and tested.[3,4]

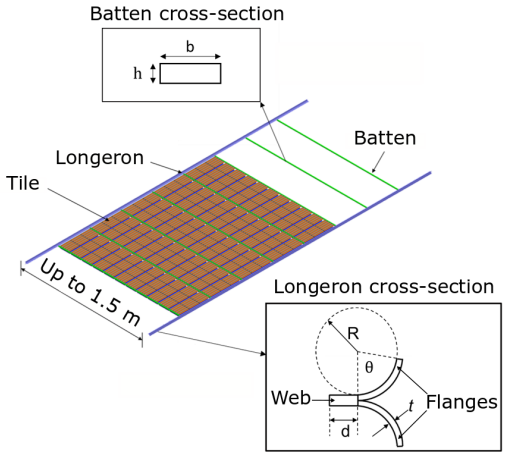

Figure 1: Overview of the ladder-type structure for the Space-based Solar Power Project.

*PhD Candidate, Graduate Aerospace Laboratories at the California Institute of Technology (GALCIT), 1200 E California Blvd. MC 205-45. froyer@caltech.edu

†Joyce and Kent Kresa Professor of Aerospace and Professor of Civil Engineering, Graduate Aerospace Laboratories, California Institute of Technology (GALCIT), 1200 E California Blvd. MC 105-05. AIAA Fellow. sergiop@caltech.edu

The ladder-type structure consists of two triangular rollable and collapsible (TRAC)[6] longerons, connected transversely by rods (battens). For the rest of the paper, this structure is referred to as a strip. In the proposed spacecraft architecture, the strip is simply supported at the ends with boundary conditions that do not allow any tension to be applied to the strip. For the specific strip considered here, the battens are rectangular cross-section carbon fiber rods and the longerons are thin composite shells. In orbit, the structure will be subjected to solar pressure and hence here we will be focusing on pressure loading for the strip.

The purpose of the present study is to understand the buckling and post-buckling behavior of a strip, and explore the sensitivity of its transition to buckling, considering the effects of disturbances and imperfections. The stability of the pre-buckling (fundamental) path is assessed and insights into early transitions into the post-buckling regime are gained by using localized probing to apply a perturbation to the structure. The probing technique is then generalized to higher order bifurcations arising from the post-buckling path. Low energy escape paths into buckling that cannot be predicted by a classical eigenvalue problem are identified. This research builds on recent advances in shell buckling and applies the tools developed for cylindrical and spherical shell buckling to the more specific problem of the strip buckling under pressure.

II. General stability landscape approach to thin shell buckling

Recent work on thin cylindrical and spherical shell buckling has focused on the stability of the buckling phenomenon and its sensitivity to disturbances. Rather than seeing buckling purely as a bifurcation problem, these new contributions have studied in more detail the meta-stability of the structure's fundamental path and the early transition into adjacent post-buckling paths requiring a small energy barrier to be overcome. A thorough review of these recent advances has been presented by Groh et al.[7]

Here we focus on one specific approach to shell buckling and the use of a new tool to study this phenomenon: the buckling stability landscape. The notion of a stability landscape was introduced by Virot et al[8] as a way to characterize the meta-stable nature of cylindrical thin-shell buckling. A local radial displacement is imposed on a compressed cylinder using a small ball probe (called "poker" in[8]) which creates a localized single dimple. The stability landscape is the surface created when the probe force is plotted as a function of the main loading (axial compression on the cylinder) and the probe displacement. It provides a very useful way to quantify the impact of probing on the buckling behavior and a general way to study the structure's buckling sensitivity to disturbances.

Even though the stability landscape was introduced in the case of thin shell cylinder buckling, a similar landscape can be found in other types of shell buckling problems. A thin shell buckling stability landscape is sketched in figure 2a. The features of this landscape and their significance, described in[8] are briefly summarized next.

- Point of spontaneous buckling. This point corresponds to a zero probe displacement and the associated load is the non-linear buckling load. At this point, no disturbance is needed at this point for the structure to transition into its post-buckling regime.

- Minimally buckled state. It corresponds to the point below which no buckles can be formed in the structure. The associated load is referred to as "Maxwell load",[9] above which the structure's pre-buckled state become meta-stable. The Maxwell load corresponds to the load for which the probe force first falls to zero for a non-zero probe displacement. It has been shown that this load can serve as an accurate bound for experimental buckling loads.[7,10]

- Buckled equilibria solutions. These states of equilibrium correspond to the zero probe force contour (for a non-zero probe displacement). Two set of solutions branch from the minimally buckled state: a stable and an unstable branch. In a load-controlled experiment, the structure will dynamically snap to the stable equilibrium path once the probe displacement reaches the unstable equilibrium path.

- Valley. This feature of the landscape is formed by the local minima of probe force and leads to the minimally buckled state.

- Ridge. It corresponds to local maxima of the probe force and forms an energy barrier between unbuckled and buckled states as shown in figure 2b. Quantifying the energy barrier is of great interest since it is directly related to the sensitivity of the structure's buckling to disturbances. This behavior is often

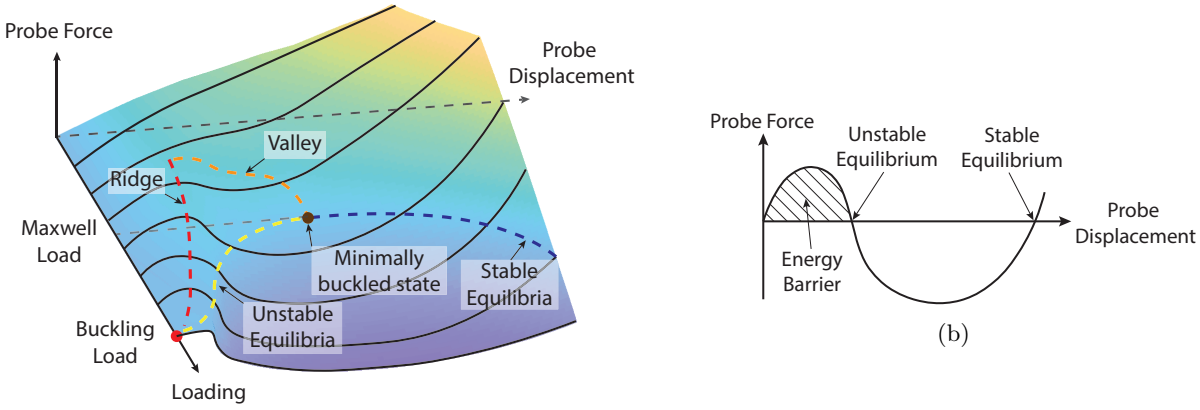

(a) (b)

Figure 2: (a) Schematic of thin-shell buckling stability landscape. Inspired from [1].(b) Energy barrier formed between pre-buckled and post-buckled state.

referred to as "shock-sensitivity".[11] Note that the point of intersection between ridge and valley marks the appearance of negative stiffness. At this point, kinetic energy (snapping) would be released in a load-controlled probing experiment.

Section III of this paper presents numerical computation of stability landscapes for the specific strip structure and section IV extends the use of these landscapes to the post-buckling regime. In section V the effect of the strip length on the stability landscape is investigated. In section VI, we generalize the probing to the entire structure which unveils the existence of low energy escape paths into buckling, similar to the ones observed for the cylinder and the sphere. Finally, section VII present a preliminary analysis on the effect of geometrical imperfections on the strip stability landscape.

III. Computation of stability landscape

III.A. Finite element model

We developed a finite element model (FEM) of strip structures, composed of two longerons of length L ranging from 1.8 m to 4.2 m. The geometry of the structure is described in figure 1. The longeron has a TRAC cross-section. The opening angle is 100 deg, the radius R is 12.2 mm, the shell thickness is $t = 98$ μm and the web length is $d = 8$ mm. The two longerons are connected by regularly spaced transverse rods called battens. The batten spacing is $S = 0.3$ m, the batten length is $W = 0.2$ m, and each batten has a rectangular cross-section with width $b = 3$ mm and height $h = 0.6$ mm. The FEM is built using the Abaqus commercial software. The longerons are modeled with 4 node reduced integration shell elements (S4R) and the battens with linear 3D beam elements (B31). The longeron flanges are made of a [45 GFPW / 0 CF /45 GFPW] laminate, often referred to as FlexLam,[12] connected with a ply of glass fiber plain weave at the web.

III.B. Finite element analysis

The structure described previously is constrained in a simply supported condition, as shown in figure 3. The outer web edge (highlighted in orange) on one of the longeron cross-sections is preventing from translating while the web edge of the other end cross-sections are constrained in a way that allows the projected strip length and projected strip width onto the (xz) plane to vary as the strip deforms.

A uniform pressure is applied on the longeron webs and on the battens top faces. The total area loaded by pressure in the numerical model is A_{BL} and the associated buckling pressure is called P_{cr-AB}. However,

in the actual spacecraft, the loading (solar pressure for instance) would be applied on the entire area A spanned by the functional elements, which can be approximated by $L \times W$. The actual buckling pressure on A is P_{cr}. In order to draw practical conclusions, all results are presented in terms of P_{cr}, using the relation $P_{cr} \times A = P_{cr-AB} \times A_{BL}$.

In addition, for each value of P, we probe the top edge of the longerons by applying a transverse nodal displacement U_{xp} at location $Z = Z_p$, and we extract the probe reaction force. Our two independent control parameters are thus the pressure and the probe displacement.

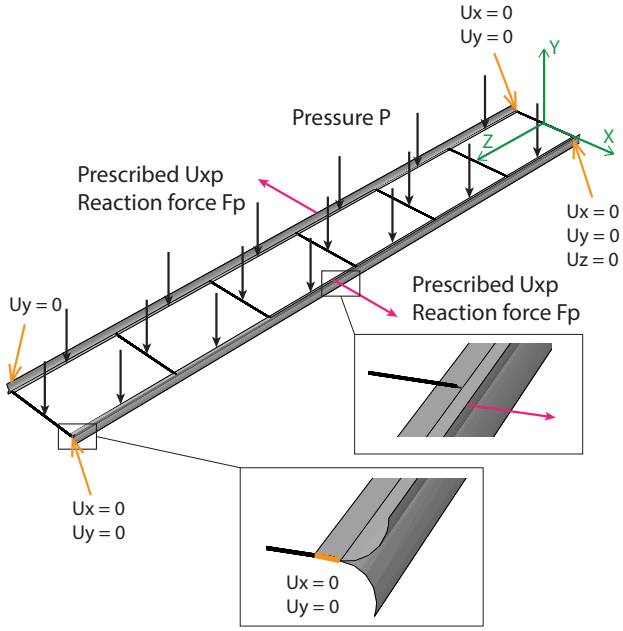

Figure 3: Schematic of finite element model used to study the strip under pressure.

The last important consideration is the choice of the probe locations. In a classical buckling and post-buckling analysis, one would compute non-linear eigenmodes and seed a linear combination of these modes into the structure's initial geometry.[13] The use of an arclength solver (the Riks method for instance) coupled with the imperfect geometry enables tracing the first bifurcation branch. We focus first on studying the early transition into such a branch, governed by the structure's non-linear eigenmodes. Therefore, the probing location will first be chosen as the location at which the peak deformation for the first eigenmodes is reached.

The first non-linear buckling eigenmodes are obtained using the following iterative scheme. A first buckling mode prediction is performed for the undeformed structure which gives us the linear buckling load P_{cr-lin}. Then pressure is applied on the strip with a magnitude equal to 50% of P_{cr-lin}. A buckling prediction is then performed on the prestress strip and a new value of the critical buckling load is then computed. This process is repeated until the pressure applied before the buckling prediction step converges to the non-linear buckling pressure. This procedure unveils 4 closely spaced eigenmodes shown in figure 4a. They consists of single dimples localizing on both sides of the central batten. The highly localized nature of these eigenmodes could be explained by the pressure loading creating a non-uniform bending moment along the strip length, the maximum magnitude being at the center of the structure. In order to study early post-buckling branches associated with such modes, the probe location is chosen as the location of maximum displacement for these modes.

In this paper, we consider two ways of probing, illustrated in figure 4b. The antisymmetric probing scheme uses one probe per longeron. The location of this probe matches the peak displacement of the first buckling mode for each longeron. The symmetric probing scheme uses 2 probes per longeron, and the probe locations are given by the location of peak displacement for the first 2 buckling modes. For both probing schemes, the probes are displaced in the strip transverse direction, in an outward direction. Note that the computed modes are combinations of inward and outward flange deflections. By conducting a classical post-buckling analysis based on a linear combination of these modes seeded in the perfect geometry, we observed that the deformed shape obtained on the first bifurcation branch featured only outward buckles. This motivated the outward probing scheme. However, by restricting the chosen probing scheme to these

modes, we are only studying the meta-stability of a specific kind of solution, but we have no guarantee that this approach yields the easiest transition into buckling. A more complete set of probing schemes would be needed to have a full picture of the complex buckling behavior of such structure. This will be the topic of future studies. A more general approach, that does not use the eigenmodes to choose the probing location is presented in the last section of the paper.

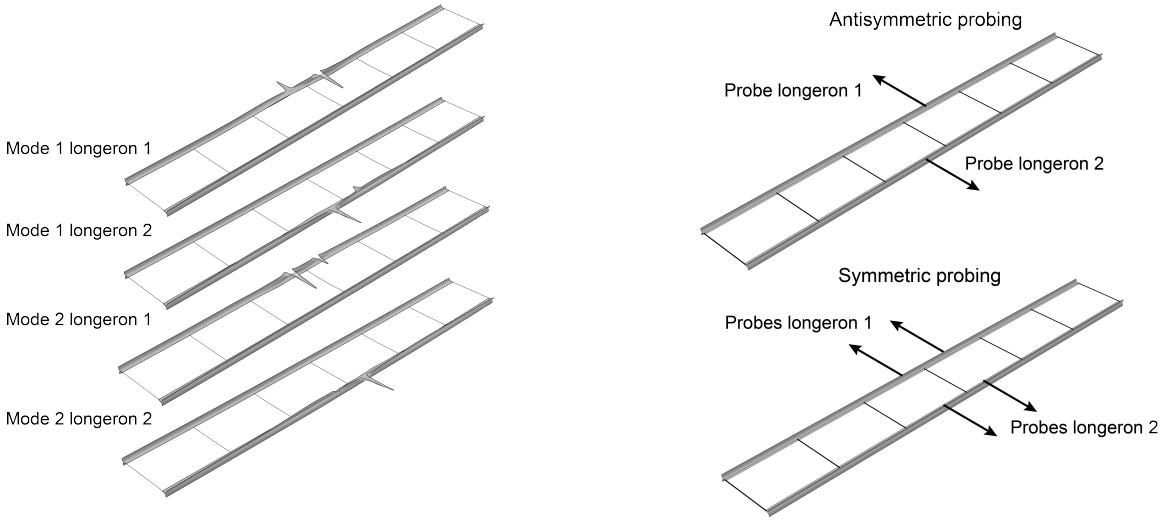

(a) (b)

Figure 4: (a) First 4 non-linear buckling modes for L = 1.8 m. (b) Symmetric and antisymmetric probing schemes derived from these modes.

III.C. Strip stability landscape

The plot of probe reaction force as a function of bending moment and probe displacement is the stability landscape for the strip. We focus in this section on a 3 m long strip for which the stability landscape is shown in figure 5. It is shown here for the antisymmetric probing scheme but the landscape for the symmetric probing scheme is very similar. We observe all the features described in the Introduction, and the behavior obtained is of the same nature as the buckling of a cylinder or sphere. The obtained Maxwell load for this specific strip length is $P_M = 0.86$ Pa. The ridge, fundamental path and unstable equilibrium contour intersect at the non-linear buckling load $P_{cr} = 1.45$ Pa.

The values of critical probe displacement obtained here are very similar to the number experimentally determine for the cylinder case.[8] However, since the longeron cross-section is open, the ridge probe force magnitude is very small. The experiment on industrial cylindrical cans[8] reported ridge forces right past the Maxwell load of about 1 N, whereas these forces falls two orders of magnitude lower here. The energy barrier required to reach the buckled equilibrium solutions after the Maxwell load is reported at the bottom of figure 6b. It falls very rapidly after the Maxwell load and reach values around 10^{-4} mJ after a pressure of 1.2 Pa is applied. The stability of the fundamental path after this pressure is extremely uncertain and we will most likely never reach the non-linear buckling load in an experiment.

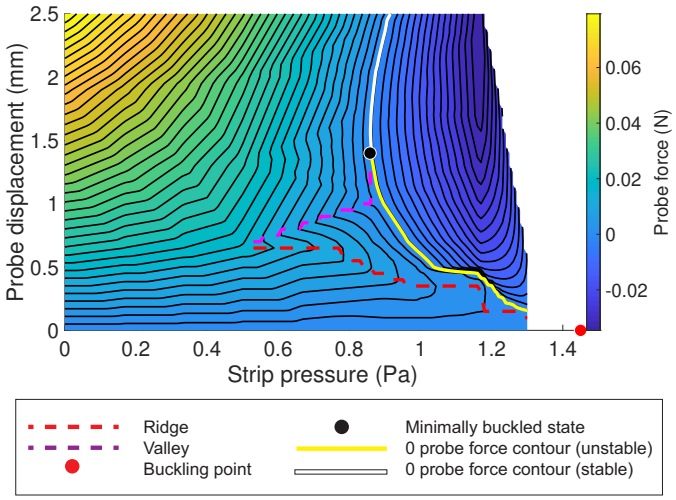

Figure 5: Computed stability landscape for a strip structure for the antisymmetric probing scheme.

IV. Generalization of stability landscapes to post-buckling regime

IV.A. Iterative construction of higher order stability landscapes

This section focuses on the determination of the ultimate pressure that can be carried by the structure. The post-buckling response of the structure needs to be studied. If we accept localized buckles forming on the longerons during operation, we could operate the structure in its elastic post-buckling regime. The post-buckling behavior is studied here using stability landscapes.

By identifying the unstable equilibrium solutions, shown in yellow in figure 2, we determine the critical probe displacement needed to reach this contour. Past this critical displacement, the probe can be released and the structure will naturally snap into the stable equilibrium solutions shown in white in figure 2. Once the stable equilibrium contour is attained, the structure has transitioned into its post-buckling path. This procedure can be implemented very easily in the finite element analysis.

Note that this methodology differs from the classical approach which consists in seeding imperfections into the structure's undeformed geometry and uses an arc-length solver (modified Riks method for instance) to force the bifurcation into a specific branch. While the classical methodology is useful to have a first order idea of the structure's post-buckling behavior, it can be quite difficult to implement. Indeed, one does not have a priori control over when the imperfect structure will bifurcate, and the post-buckling path is approximate since the structure's geometry has been changed. For imperfection sensitive structures (almost all thin shell structures), these two effects are particularly pronounced and it becomes quite hard to resolve higher order bifurcation paths (bifurcation from the primary post-buckling branch) since the imperfection needed to resolve the higher order bifurcations can modify the structure's behavior for earlier bifurcations. Path following methods[14] are extremely powerful and would allow the exact post-buckling path for this structure to be traced. However these methods are usually not available in commercial finite element codes. The advantage of using the probing method adopted here is that it gives insights into the stability of the fundamental and post-buckling paths and their resilience to disturbances, while allowing to resolve the strip behavior after multiple bifurcations, and thus up to the ultimate failure pressure.

Once the structure starts following its first post-buckling path, the behavior can be determined until a new bifurcation is encountered. At this point, a non-linear eigenvalue computation can be performed and the probing process can be repeated using the maximum amplitude location of these new eigenmodes to determine the new probing location. Note that once the $n-1$ buckle is fully formed, there is no more need to continue probing at its location and the $n-1$ probe can be released as the n probe is active. This iterative process is repeated until the maximum pressure is found. The result of this process is illustrated in figure 6, corresponding to the antisymmetric probing of figure 7a. A specific post-buckling path is shown but there exists an infinite set of other possible paths. For each path, we can associate a specific level of disturbance and the associated energy barriers are reported in figure 6b. However, while the probing pressure

sets the pressure at which the transition occurs, it does not affect the behavior of the structure once the stable equilibrium path is reached. It means that for a specific probing scheme, the maximum pressure will be independent of the path chosen. Finally even if a buckle is fully formed and no probe is applied, we can continue tracking the buckle peak displacement. The free peak displacement of the 3 buckles is shown in black in figure 6. We can notice that buckle 1 yields the largest deformation. Global failure of the strip occurs when buckle 1 reaches a maximum value of outward displacement for P_{max}. At this point, a localized fold forms at the center of the structure while the amplitudes of buckle 2 and 3 decreases, and the strip starts folding.

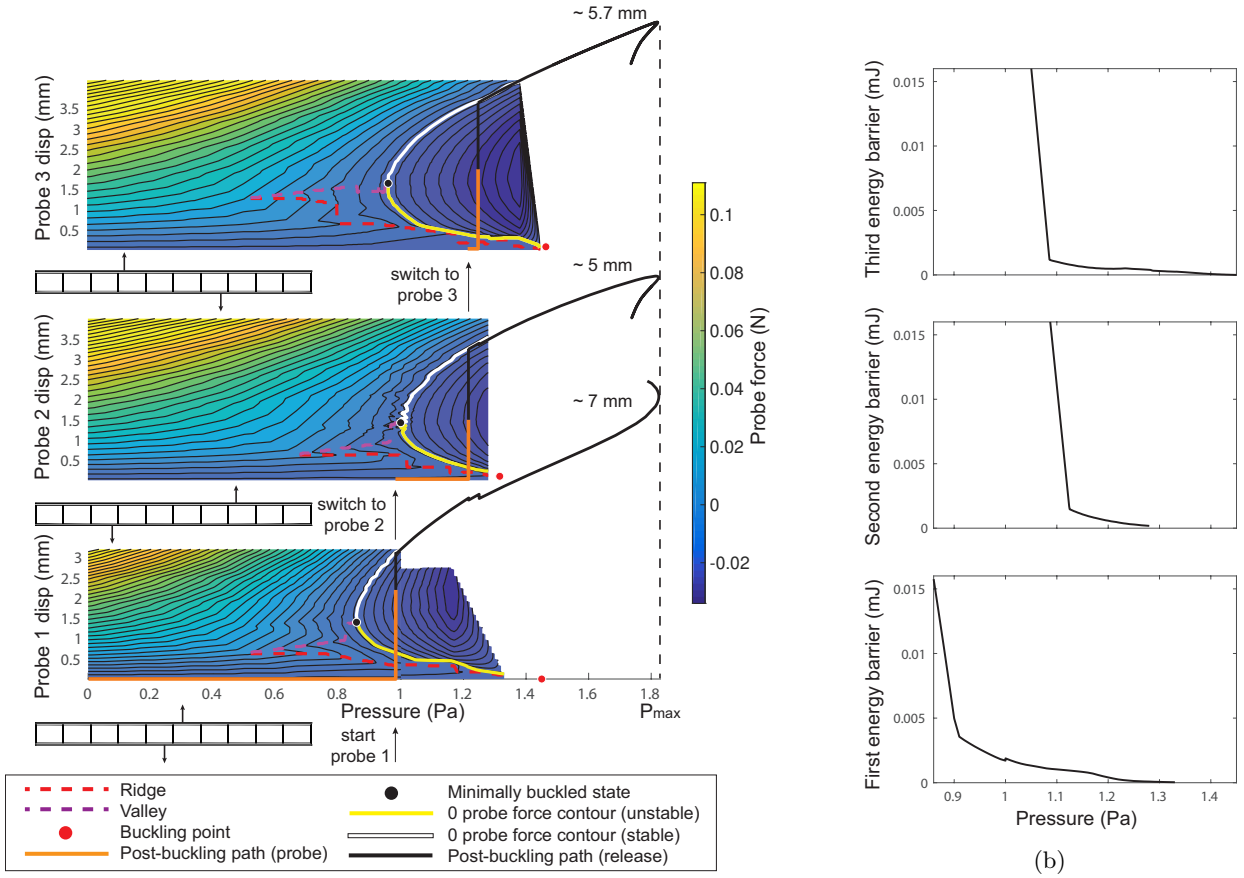

(a) (b)

Figure 6: (a) Stability landscapes obtained for the first, second and third transitions into buckling.(b) Energy barriers between pre-buckled and post-buckled states for each of the 3 buckling transitions.

IV.B. Post-buckling response for symmetric and anti-symmetric probing

The method described in the previous subsection is used to trace the structure's post-buckling response for symmetric and anti-symmetric probing. The antisymmetric probing starts as described in figure 4b. The subsequent probes 2 and 3 are determined using the iterative method described earlier taking only the first eigenmode for each longeron. Similarly, the symmetric probing starts as described in figure 4b and takes the first two eigenmodes as probe locations, which results in using 4 probes at a time. These two iterative probing schemes are shown in figure 7a.

The probing approach allows to trace the full post-buckling response shown in figure 7b. The x axis corresponds to the displacement extracted in the middle of the longeron (1.5 m from the end), at the cross-section centroid. The failure of the structure, described earlier also appears as an horizontal tangent in this plot, which highlights the loss of stiffness at the maximum value of pressure. Notice that the antisymmetric probing scheme yields a softer post-buckling regime and lower value of the maximum pressure. It is thus the

probing scheme that an engineer should consider when determining safe bounds on the structure's range of operations.

In addition to the probing method, an attempt has been made to compute the full antisymmetric post-buckling response using the "traditional" method which consists in seeding the buckling modes shapes into the initial geometry. The result is shown with a black dashed line with a total imperfection amplitude of 2%. The probing and "traditional" techniques give the exact same result for the first post-buckling branch. However, we were not successful in going past the first post-buckling regime. Due to the structure's high imperfection sensitivity, seeding the second buckling modes in the initial geometry (even for an imperfection amplitude of less than 0.5% of the shell thickness) degrades the pre-buckling response and we are no longer able to resolve the first bifurcation. Finally, with the numerical probing technique presented in this paper, the structure transitions from its fundamental path directly to the stable post-buckling branch while the applied pressure is kept constant. Such scheme while numerically efficient will not detect any potential bifurcations arising from the unstable post-buckling branch, as highlighted by Pirrera et al.[15] Such bifurcations could give rise to different stable post-buckling branches.

To overcome this limitation, two approaches are taken. The first one consists in checking the tangent stiffness matrix eigenvalues as the structure is probed. Any intersection with a new stable post-buckling branch will be detected. The probing scheme can then be changed following the eigenmodes of this new bifurcation, before reaching the stable equilibrium contour of the previously determined bifurcation branching from the fundamental path. However this approach will not be able to detect unstable paths that do not restabilize since they do not intersect with the probing path. The second approach consists in stopping the probing right before reaching the unstable equilibrium contour. The full unstable and stable branch can then be resolved using an arclength solver and one can directly check for 0 eigenvalues on the unstable post-buckling branch. This second technique has been used successfully for a different type of structure and will be the subject of a future paper. For the ladder-type coilable structure we did not detect any 0 eigenvalues while probing, and preliminary experiments suggest that there are no fully unstable paths leading to early failure before the ultimate pressure is reached.

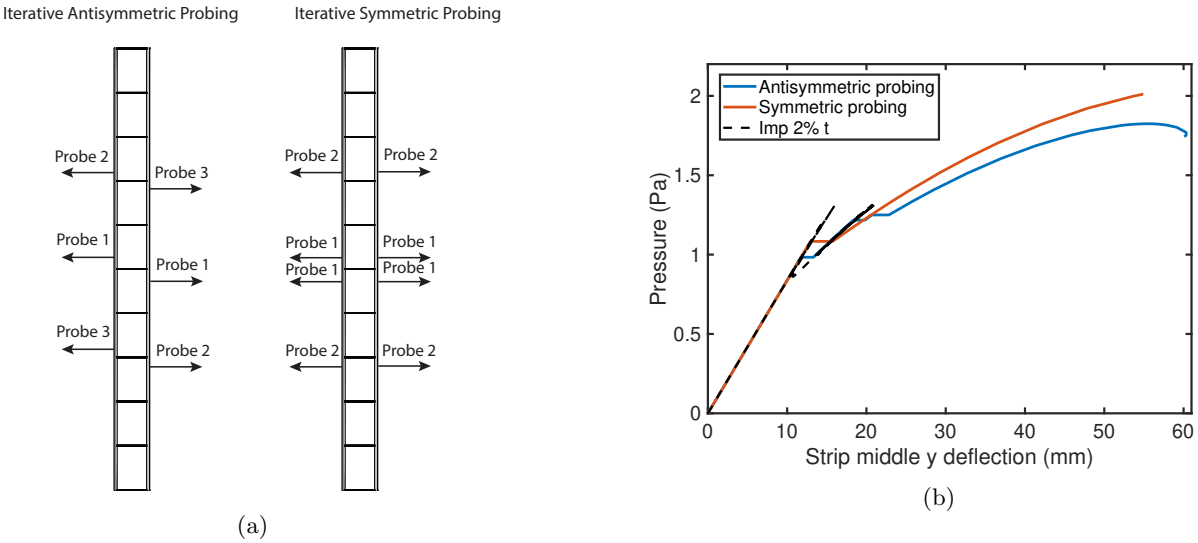

Figure 7: (a) Probing schemes derived from the iterative constructions of stability landscapes.(b) Full post-buckling response for the symmetric and antisymmetric probing scheme.

V. Effects of strip length on buckling energy barrier and characteristic loads

The analysis described in section II-A has been repeated for strip lengths of 1.8 m, 4.2 m, 5.4 m and 6.6 m. The first quantity that has a direct impact on the early buckling of the structure is the Maxwell load and we computed it for all the considered strip lengths. We also track the evolution of the linear and non-linear buckling pressure. Finally, by computing the full post-buckling response of the structure, we also determined the ultimate buckling load. The evolution of these 4 quantities as a function of the strip length

is shown in figure 8a.

Both the linear and non-linear buckling pressures decrease as the strip length increases. The linear buckling pressure (eigenvalue problem for the undeformed structure) slowly converges to the non-linear buckling pressure (from section III.B) and this is also visible in the eigenmodes. While non-linear modes localized on the side of the central batten, the linear mode is purely symmetric with respect to the central batten. As the length of the strip increases, the non-linear buckling modes become less and less localized and more symmetric with respect to the central batten. This is shown in figure 9.

Our second observation is that the ultimate buckling pressure also decreases as L increases. When looking at the formation of local buckles in the post-buckling regime, we observe that the longer the strip, the more buckles are formed before reaching the ultimate buckling load. Since the formation of a buckle in the structure is associated with a decrease in stiffness, the structure will reach a zero value of stiffness earlier if more buckles can form, since the Maxwell load for higher order buckles does not increase significantly (see section IV.B). It gives an intuitive way of understanding this decrease in maximum pressure. The ultimate buckling load is about 1.39% greater than the non-linear buckling load for $L = 1.8$ m and becomes 1.26% greater for $L = 4.2$ m.

We observe a similar decrease in Maxwell load as L increases. Notice that the ultimate buckling load converges faster to the non-linear buckling load than the Maxwell load.

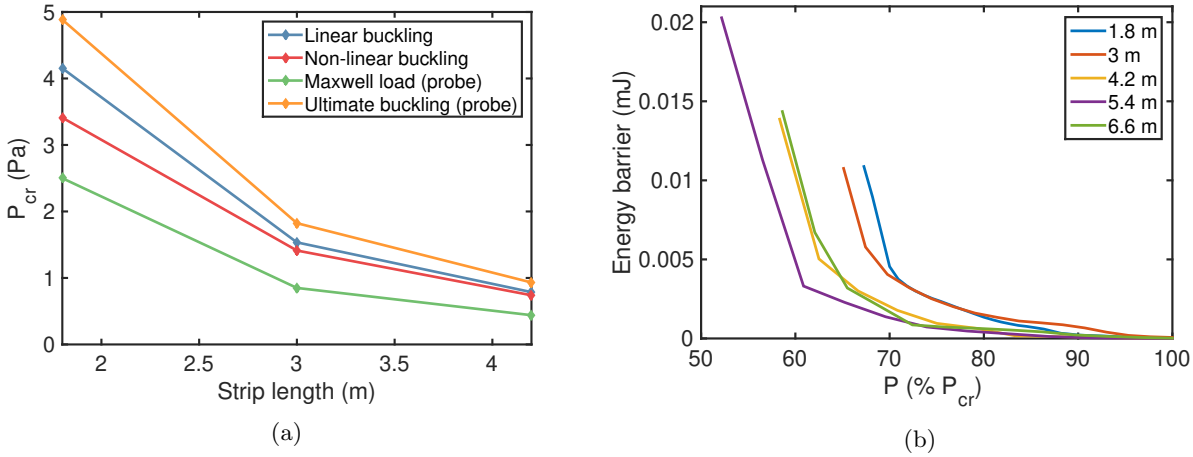

(a) (b)

Figure 8: (a) Evolution of the structure's critical loads as a function of L. (b) Evolution of the energy barrier as a function of L.

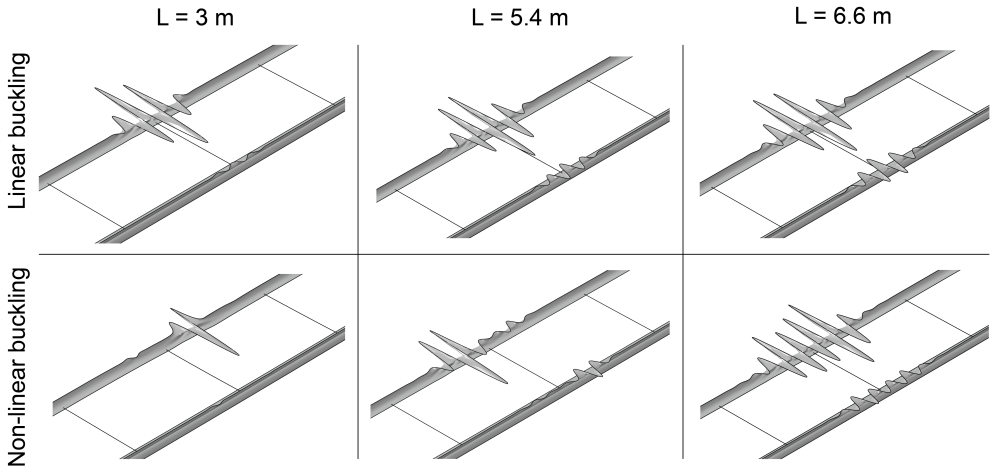

Figure 9: Comparison between linear and non-linear buckling mode shapes for 3 different lengths.

The energy barrier for early buckling into the antisymmetric first mode branch is reported for the various

strip lengths considered in figure 8b. The shape of the barrier is consistent across lengths and follows qualitatively the same trend as the Maxwell load. For lower Maxwell loads, the meta-stable region of the fundamental path starts earlier and the energy barrier decreases at a specific value of pressure (relative to the critical buckling load). A surprising effect arises when the strip length increases. The Maxwell load (origin of the energy barrier) and energy barrier decreases when L increases up to $L = 5.4$ mm. However when L is increased further to 6.6 m, the opposite trend is observed: the Maxwell load and energy barrier increase to values matching $L = 4.2$ m. This indicates that the Maxwell load and energy barrier are not monotonic with respect to the strip length.

VI. Search for low energy escape paths

VI.A. Existence of broken away paths

We previously studied early transitions into post-buckling for the first classical non-linear buckling modes. These were determined solving iteratively an eigenvalue problem until converging to the non-linear buckling load. However, while these modes give rise to a meta-stable fundamental path above the Maxwell load, we are not guaranteed that they actually constitute the easiest escape into buckling. There may exist some broken away paths in the immediate vicinity of the fundamental path associates with a very low energy barrier, which would yield an earlier transition into post-buckling or a softer structure in the post-buckling regime. Such paths have been recently studied extensively for the case of the cylindrical shell under axial compression and for the spherical shell under pressure.[17,18] For the cylinder case the corresponding mode shapes take the form of a localized dimple. These paths run asymptotically close to the fundamental path without ever intersecting it, and thus no bifurcations can be predicted using a traditional eigenvalue problem.[16] The points forming this path are referred to as mountain pass points, because they corresponds to the top of a ridge in the total potential energy map. This ridge separates the fundamental well from a lower potential well corresponding to localized buckling modes, and these points correspond to the unstable equilibrium contour on the probe force stability landscape. There may exist an infinite number of such broken away paths but the focus has been on finding the easiest escape route into buckling and thus on the mountain pass point requiring the least amount of energy to be reached. This point is called lowest mountain pass point and it has been shown that the single dimple solution is indeed the lowest mountain pass point for the cylinder.[19] In this paper we are interested in determining whether such mountain pass points exist for our specific structure.

VI.B. Extending probing to the entire structure to unveil mountain pass points

In order to search for broken away paths and mountain pass points, the finite element analysis described in section II.B has been extended to multiple probe locations. For $L = 3$ m, the top edge of each longeron is discretized into 39 different probe locations (one probe location every 75 mm) along the strip axis and are located by their Z coordinate. Both longerons are probed in the same outward anti-symmetric fashion as described in section IV.A, but the probe location Z from the strip end is changed for each new analysis. The probe force is extracted for each probe location and for different values of the applied pressure. For each combination of pressure and probe location, a value of energy barrier is computed as described in the introduction. A triangulation-based linear interpolation is used to determine the energy barrier for values of probe locations and pressures between our simulated values.

The energy barrier is plotted as a function of the probe location Z and the applied pressure. The resulting energy barrier map is shown in figure 10a. We first focus on pressures close to the non-linear buckling load. For these pressures, 3 energy barriers are reported in figure 10b. The energy barrier is very close to zero and the local minimum of the energy barrier is reached at Z locations corresponding to the first buckling modes ($Z = 1423$ mm and $Z = 1479$ mm). These locations correspond to the first zero energy barriers. However one can see that there exist other local minima further away from the center of the strip ($Z = 1120$ mm and $Z = 1880$ mm). For $P = 1.167$ Pa, these local minima are relatively high compared to the buckling mode minima but they quickly drop to similar values for $P = 1.33$ Pa.

This suggests that buckling could occur at these locations for a minimal disturbance, in addition to or instead of the locations predicted by the eigenvalue problem. However, the buckling modes are still giving the lowest energy barrier strictly speaking. This is no longer the case when looking at lower values of pressure in figure 10a. Indeed we observe global minimum of energy barrier at locations different from the

first buckling modes. For $P = 0.96$ Pa, we observe a global minimum for the energy barrier at the center of the strip ($Z = 1500$ mm) surrounded by two local minima at $Z = 1282$ mm and $Z = 1722$ mm. The global minimum changes location rapidly and for $P = 0.98$ Pa, we observe global minima at locations $Z = 1202$ mm and $Z = 1802$ mm. We verified that the pressure is above the Maxwell load for probing at these locations, which means that buckled equilibrium solutions exist at these locations. None of these buckling locations are predicted by solving the eigenvalue problem and they are mountain pass points for the outward antisymmetric probing scheme. A very important observation is that the lowest mountain pass points for our structure depend on the pressure. Finally, we only focused on the antisymmetric probing scheme here but we expect that even lower mountain pass points could be obtained if only one longeron is probed locally. This conjecture has to be verified and will be the topic of a future paper.

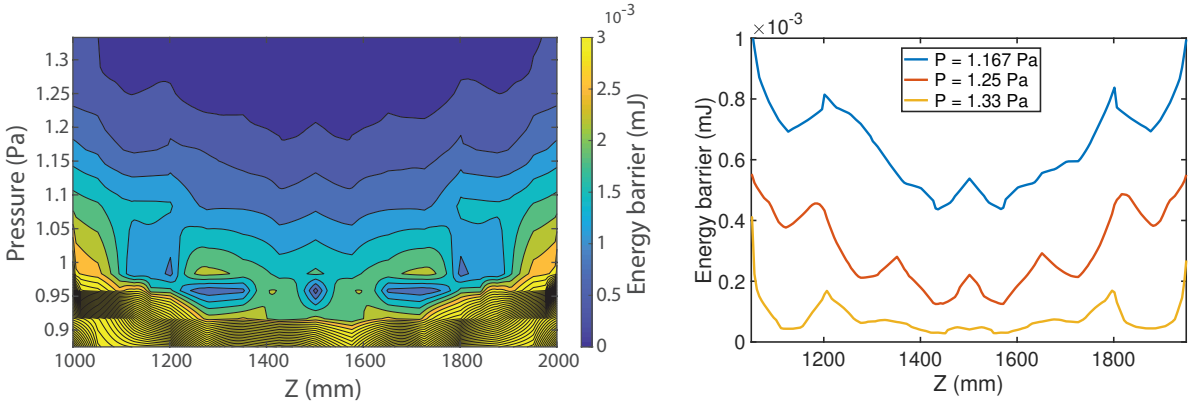

Figure 10: (a) Plot of energy barrier vs. strip z location vs. pressure.(b) Detail of 3 high pressure energy barriers.

VII. Effect of initial imperfections on strip stability landscape

One essential aspect to consider when dealing with thin shells is their sensitivity to geometric imperfections. We are especially interested in quantifying the impact that imperfections in the undeformed geometry have on the structure's stability landscape and early buckling. For this specific study we have restricted our analysis to the case $L = 1.8$ m and we have considered one specific imperfection based on the first eigenmode for longerons 1 and 2, shown in figure 4a. While a more thorough investigation would be needed to fully assess the effect of a wider range of imperfections, this study serves as a starting point to qualitatively understand the sensitivity of the stability landscape features.

The imperfect structure is probed using the outward antisymmetric probing scheme at the location of peak buckling mode displacement. In this specific case, the probing location also corresponds to the location of maximum imperfection amplitude. The imperfect amplitude is expressed in terms of shell thickness (t). We consider amplitudes ranging from 0% t to 50% t. The stability landscapes obtained for this specific probing scheme and the set of imperfection amplitudes considered are shown in figure 11a.

We first notice that the imperfection has a significant impact on the structure's buckling load, which corresponds to the pressure above which the stability landscape can no longer be computed (the solver encounters the first bifurcation). For the perfect geometry, the buckling pressure is $P_{cr} = 3.3$ Pa which decreases to 2.9 Pa (88% of P_{cr}) for an imperfection amplitude of 10% t, 2.48 Pa (75% of P_{cr}) for an imperfection amplitude of 30% t to finally reach 2.08 Pa (63% of P_{cr}) for an imperfection amplitude of 50% t. The second important observation is that the Maxwell is barely affected by the imperfection for an amplitude under 40% t. For the perfect geometry, the Maxwell load is $P_M = 2.26$ Pa. This does not change for an imperfection of 10% t and slightly decreases to 2.22 Pa and 2.2 Pa for an imperfection amplitude of 30% t and 40% t respectively. For a critical value of imperfection amplitude between 40% t and 50% t, the buckling load equals the Maxwell load and past this value of imperfection, the structure is not meta-stable anymore. The third feature of interest is the energy barrier required to reach early buckling for the imperfect structure, is shown in figure 11b. We observe a decrease in energy barrier as the imperfection amplitude

increases. We observe a sudden drop in energy barrier for imperfection amplitudes above 10% t.

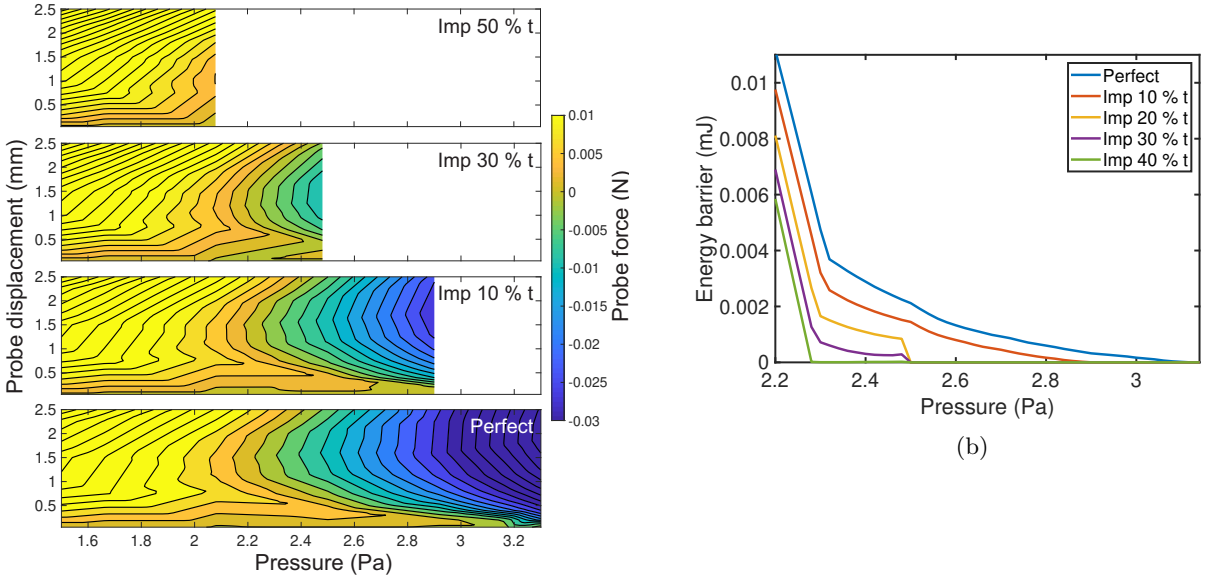

(a) (b)

Figure 11: (a) Evolution of the 1.8 m strip stability landscape for antisymmetric probing with growing geometrical imperfections.(b) Evolution of the first buckling energy barrier for the 1.8 m strip with growing geometrical imperfections.

VIII. Conclusion

This paper has presented numerical results exploring the buckling and post-buckling behaviors of an ultralight ladder-type coilable space structure, used as a building block for large area deployable spacecraft. This thin shell structure is different from classical thin shell structures such as the cylindrical shell or the sphere,and the loading considered here is very specific to our application and different from what has been studied previously. We have shown that the buckling behavior for such a structure is very similar to the one found in the more classical structures. Specifically, we studied the response of the ladder-type structure when a localized disturbance is introduces using probe forces, following recent work on the cylinder and the sphere. We showed that a similar stability landscape exists for early transition into the predicted buckling modes and that the conclusions reached for the cylinder and sphere also apply for this specific problem. In addition we showed that using probing forces provides an effective way to derive the full stable post-buckling response and gain insight into the meta-stability of the post-buckling path. It is especially useful when multiple successive buckles are encountered as it provides insight into the level of disturbance needed to form specific series of buckles. We further extended the probing to any location on the structure's longerons. This analysis unveiled the existence of broken away paths (mountain pass points) similar to the single dimple found for the cylinder and sphere, and that the mode shapes for these specific early buckling paths localize at different locations than the ones predicted by a classical eigenvalue problem. The important take away for this problem is that the location of the lowest mountain pass point (minimum energy barrier to transition into buckling) is a function of pressure. Finally, the effect of imperfections based on the first buckling mode on the strip stability landscape has been assessed. While the imperfections degrade the buckling load significantly, and erode the energy barrier separating pre-buckled and post-bucked states, it seems that it has very little impact on the Maxwell load. For a specific value of imperfection amplitude, the buckling load

reached the Maxwell load and the structure loses its meta-stability.

As far as the engineer is concerned, this new extension of probing approach to the study of more complex structures enables different design strategies. If the application requires buckling to be avoided, the structure can be designed such that it never exceeds the Maxwell load. If upper bounds on disturbances amplitude during operation and manufacturing deviations are thoroughly quantified, the structure can be operated above its Maxwell load by using the energy barrier of the worst imperfect structure as main design limit. Finally, in the case of a stable post-buckling regime and if small buckles are accepted during operation, the ultimate failure load can then be derived efficiently using the probing technique and can be used as a design criterion.

The specific prototypes we are building currently[4] can be analyzed using this framework. For 0.2 m wide strip, and for lengths ranging from 1.5 m to 4.2 m, our structure will have critical pressures ranging from 5 Pa to 1 Pa at which the structure will elastically collapse by folding around its center. The Maxwell loads ranging from 2.5 Pa to 0.5 Pa are orders of magnitude greater than the solar pressure the structure would experience in orbit. However, earlier studies showed that the non-linear buckling pressure of these structures and the solar pressure are of the same order of magnitude for strip lengths above 40 m. For these long strips, the knowledge of the strip stability becomes crucial and the method presented in this paper would play a key role in enabling the design of such large spacecraft structures.

Acknowledgments

Financial support from the Space Solar Power Project at Caltech is gratefully acknowledged.

References

[1]Goel, A., Lee, N. and Pellegrino, S. (2017). Trajectory design of formation flying constellation for space-based solar power. IEEE Aerospace Conference, Big Sky, MN

[2]Arya, M., Lee, N. and Pellegrino, S. (2016). Ultralight structures for space solar power satellites. SciTech 2016, San Diego, AIAA-2016-1950

[3]Gdoutos, E., Leclerc, C., Royer, F., Turk, D.A., and Pellegrino, S. (2019). Ultralight spacecraft structure prototype. SciTech 2019, San Diego (CA), AIAA-2019-1749

[4]Gdoutos, E. E., Truong, A., Pedivellano, A., Royer, and Pellegrino, S. (2019). Ultralight deployable space structure prototype. SciTech 2020, Orlando (FL)

[5]Royer, F. and Pellegrino, S. (2018). Ultralight ladder-type coilable space structures. SciTech 2018. Orlando (FL), AIAA-2018-1200

[6]Murphey, T.W. and Banik, J., 2011. Triangular rollable and collapsible boom. U.S. Patent 7,895,795.

[7]Groh, R.M.J. , Pirrera A. 2019. On the role of localizations in buckling of axially compressed cylinders. Proc. R. Soc. A 475:20190006.http://dx.doi.org/10.1098/rspa.2019.0006

[8]Virot, E., Kreilos, T., Schneider, T.M. and Rubinstein, S.M., 2017. Stability landscape of shell buckling. Phys. Rev. Lett. 119, 224101

[9]Hunt, G.W., Lucena-Neto, E. 1993 Maxwell critical loads for axially loaded cylindrical shells. Trans. ASME 60, 702–706. (doi:10.1115/1.2900861)

[10]Gerasimidis, S., Virot, E., Hutchinson, J. W. and Rubinstein, S.M. On establishing buckling knockdowns for imperfection-sensitive shell structures. J. Appl. Mech. -85-091010-1-14 (2018)

[11]Thompson, J.M.T., Sieber, J. 2015 Shock-sensitivity in shell-like structures: with simulations of spherical shell buckling. Int. J. Bifurcation Chaos 26, 1630003. (doi:10.1142/S0218127416300032)

[12]Pollard, E. L. and Murphey, T. W. Development of deployable elastic composite shape memory alloy reinforced (DECS-MAR) structures. 47th AIAA Conference, Newport, RI: AIAA, 2006

[13]Rahman, T., Jansen EL. 2010 Finite element based coupled mode initial post-buckling analysis of a composite cylindrical shell. Thin-Walled Struct. 48, 25–32. (doi:10.1016/j.tws.2009.08.003)

[14]Groh, R.M.J., Avitabile, D., Pirrera, A. 2018 Generalised path-following for well-behaved nonlinear structures. Comput. Methods Appl. Mech. Eng. 331, 394–426. (doi:10.1016/j.cma.2017.12.001)

[15]Pirrera, A., Avitabile, D., Weaver, P.M. Bistable plates for morphing structures: A refined analytical approach with high-order polynomials. International Journal of Solids and Structures, volume 47, Issues 25–26. doi:10.1016/j.ijsolstr.2010.08.019

[16]Hunt, G.W., Peletier, M.A., Champneys, A.R., Woods, P.D., Wadee, M.A., Budd, C.J., Lord, G.J. 2000. Cellular buckling in long structures. Nonlinear Dyn. 21, 3–29. (doi:10.1023/A:1008398006403)

[17]Hutchinson, J.W. 2016 Buckling of spherical shells revisited. Proc. R. Soc. A 472, 20160577. (doi:10.1098/rspa.2016.0577)

[18]Hutchinson, J.W., Thompson, J.M.T. 2017 Nonlinear buckling behaviour of spherical shells: barriers and symmetry-breaking dimples. Phil. Trans. R. Soc. A 375, 20160154. (doi:10.1098/rsta.2016.0154)

[19]Horák, J., Lord, G.J., Peletier, M.A. 2006 Cylinder buckling: the mountain pass as an organizing center. SIAM J. Appl. Math. 66, 1793–1824. (doi:10.1137/050635778)